Annealing and Defect Trapping in Lamellar Phases of Triblock Terpolymers

Laurent Corté,[†,‡] Kazuhiro Yamauchi,[†] François Court,[§] Michel Cloître,[‡] Takeji Hashimoto,[*,†] and Ludwik Leibler[*,‡]

Department of Polymer Chemistry, Graduate School of Engineering, Kyoto University, Yoshida-honmachi, Sakyo-ku, Kyoto 606-8501, Japan, Laboratoire Matière Molle et Chimie (UMR 167), ESPCI, 10 rue Vauquelin, 75231 Paris Cedex 05, France, and CERDATO, ATOFINA, 27470 Serquigny, France

Received February 10, 2003; Revised Manuscript Received June 4, 2003

ABSTRACT: Equilibrium morphologies in molten ABC triblock terpolymers are much more difficult to attain than in AB diblocks. Here, we show that even the simplest lamellar structures exhibit high sensitivity to preparation conditions and that strongly trapped structural defects inherent to ABC triblock architecture cannot be removed by long annealing. Poly(styrene)-*block*-poly(butadiene)-*block*-poly(methyl methacrylate) (SBM) triblock terpolymers with nearly symmetric composition and low molar mass are studied by combining transmission electron microscopy with dynamical mechanical analysis and small-angle X-ray scattering. We find that annealing can induce a transition from a lamellar structure in which S and M end blocks are mixed together to a lamellar structure where all three components S, B, and M are segregated. The presence of B "loops" and B "bridges" is at the origin of characteristic defects which are difficult to eliminate. In a blend of SBM triblock terpolymer with a poly(styrene)-*block*-poly(butadiene) (SB) diblock having the same block length, diblock chains are completely incorporated in the lamellar structure obtained after solvent evaporation. However, annealing induces a macroscopic phase separation of SB and SBM chains. We propose a scenario for the separation mechanisms based on highly confined diffusion of SB chains within the SBM ordered structures.

I. Introduction

Hundreds of papers published in recent years have been devoted to block copolymer self-assembly. Theories mostly considered thermodynamic equilibrium. In practice, the observed morphologies do depend on preparation conditions. In block copolymers unlike in small molecule systems, it is often impossible to reach a disordered phase by heating without degrading the polymer. Hence, in most experiments, it has been necessary to rely on long and careful annealing of ordered phases or slow evaporation and casting from an adequate neutral solvent. It is clear and well-documented that, in many situations, neither of these methods is satisfactory. From a practical point of view, it is important to know whether and how the synthesis and extraction conditions (solvent choice, devolatilizing, etc.) influence the morphology and properties of copolymer materials. It is also relevant to understand the mechanisms of defect formation and defect annihilation. Indeed, a potential use of copolymers in new applications such as lithography, dielectric mirrors, or waveguides highly depends on the ability to produce regular structures and eliminate morphological defects.[1,2]

Our aim in this paper is to discuss some of the questions relative to equilibration mechanisms in the case of ABC triblock terpolymers. Due to the presence of a chemically different third block, ABC triblock terpolymers can self-assemble into a wide range of complex mesophases which are inaccessible to simple AB or ABA block copolymers.[3−6] Some of these morphologies arouse a lot of interest in both scientific and technological fields. However, it is not completely clear yet whether the morphologies observed in melts are equilibrium structures or are trapped metastable states. Here, we consider the simplest case of relatively low molar mass symmetric chains which should form lamellar structures. In this situation, chain diffusion is facilitated. At equilibrium, as will be discussed below, a lamellar morphology with well-separated A-, B-, and C-rich microdomains is expected. Yet, for poly(styrene)-*block*-poly(butadiene)-*block*-poly(methyl methacrylate) (SBM) triblock terpolymers, we find that the observed as-cast morphologies dramatically depend on sample history. Indeed, by playing with solvent selectivity, we could obtain a partially mixed lamellar morphology where S and M end blocks are mixed into the same lamellar microdomains.[9−11] Subsequent annealing of this metastable structure induces a microphase separation of the S and M blocks, as illustrated in Figure 1. Such morphological transformation implies some intriguing reorganization mechanisms of the S, B, and M blocks since chain diffusion is highly confined in the ordered structure and layer-to-layer permeation is strongly inhibited.[12−15] We might expect, in particular, that the presence of B "loops" and "bridges" has a

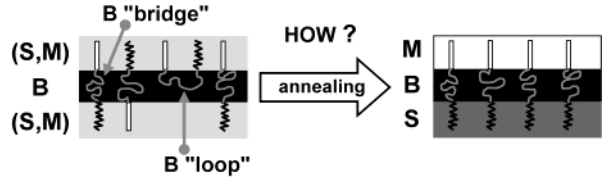

Figure 1. Transition from a partially mixed to a well-separated lamellar structure in ABC triblock terpolymers. What are the mechanisms involved?

* To whom correspondence should be addressed. E-mail: hashimoto@alloy.polym.kyoto-u.ac.jp (T.H.); ludwik.leibler@espci.fr (L.L.).
† Kyoto University.
‡ ESPCI.
§ ATOFINA.

10.1021/ma034169j CCC: $25.00
Published on Web 09/13/2003

Table 1. Characteristics of the S, B, and M Blocks, SB Diblock, and SBM Triblock

	M_n, kg/mol	M_n/M_w	T_g, °C, by DMA (1 Hz, 2 °C/min)
S block	8.8	1.2	96
B block	16		−81
M block	16		144
diblock $S_{36}B_{64}{}^{25}$	25	1.3	
triblock $S_{22}B_{39}M_{39}{}^{41}$	41	1.4	

substantial influence on structural equilibration and defect formation. The analysis of defects presented in sections III and IV seems to confirm this picture.

As mentioned above, the fact that nonequilibrium structures are easily trapped in ABC terpolymers can be a drawback in some applications. However, in some other situations, it can also be a substantial asset. Indeed, industrial block copolymer materials usually contain residual subproducts of the synthesis, homopolymers A in the case of AB diblocks or copolymers AB in the case of ABC triblocks.[16] Such mixtures most often tend to phase separate on macroscopic scales, subsequently altering the properties of the materials (transparency, mechanical strength, ...).[8,17] It would then be of great interest if one could use preparation conditions to prevent the phase separation of the residual subproducts. We study a mixture of the low molar mass symmetric SBM triblock chains with residual SB diblock copolymers coming from the incomplete copolymerization of the triblock. Surprisingly for a high diblock content (50 mol %), diblock chains are found to be completely incorporated in the SBM as-cast structure. During the structural reorganization induced by long annealing, diblock chains are expelled and a macroscopic phase separation is observed. We describe the mechanisms of this separation.

II. Experimental Section

II.1. Materials. We study a low molar mass SBM triblock terpolymer synthesized and characterized by ATOFINA. The triblock molar mass is about 40 kg/mol with a polydispersity index of 1.4. At the end of the synthesis, the material contains 36 wt % (i.e., 50 mol %) SB diblock copolymer with the same block length as SB in the SBM triblock terpolymer. This SB diblock was extracted using a selective solvent technique as already reported elsewhere.[10] The efficiency of the extraction was then checked by chromatography, and less than 1 wt % of the remaining SB diblock was detected.

To describe the copolymers, we use the $A_xB_yC_z{}^{M_n}$ or $A_xB_y{}^{M_n}$ nomenclature, where subscripts x, y, and z are the weight fractions of the components and M_n is the total number average molar mass (kg/mol). The SBM triblock and SB diblock are referenced, respectively, as $S_{22}B_{39}M_{39}{}^{41}$ and $S_{36}B_{64}{}^{25}$. For the as-prepared materials comprised of 64 wt % $S_{22}B_{39}M_{39}{}^{41}$ and 36 wt % $S_{36}B_{64}{}^{25}$, the overall composition can be described as $S_{29}B_{47}M_{24}$. As a simplification, we designate it as an SBM/SB blend in the present paper. The characteristics and glass transition temperatures (T_g) of each block are given in Table 1. The glass transition temperatures of S, B, and M were determined by dynamical mechanical analysis (DMA) (2 °C/min, 1 Hz) in films of SBM/SB blends where S, B, and M are found to be well-separated.

II.2. Sample Preparation. Films with a thickness of about 1 mm were cast from both chloroform and ethylbenzene solutions at an initial concentration of 5 wt % into covered Petri dishes. The solvents slowly evaporated at 25 °C for 2 weeks, and the films were further dried in a vacuum oven at 120 °C for 12 h. Small-angle X-ray scattering (SAXS) measurements showed that this first annealing has no significant effect on the morphology of the as-cast films with respect to the discussion given in this paper. For the sake of clarity, we consider that these samples correspond to the "as-cast" state. Parts of these films were subsequently annealed under vacuum at 170−180 °C for 4−6 h and will be referred to in what follows as "annealed" samples.

II.3. Transmission Electron Microscopy (TEM). We used the conventional transmission electron microscopy technique of stained ultrathin sections. Thin sections were cut by ultramicrotomy with a diamond knife at −80 °C and stained using osmium tetroxide (OsO_4) vapor, which selectively stains poly(butadiene) microdomains. Experiments were carried out with a JEM 2000FXZ electron microscope at an acceleration voltage of 120 kV.

II.4. SAXS. SAXS measurements were performed with an apparatus consisting of an 18 kW rotating anode X-ray generator, a graphite-crystal incident-beam monochromator, and a 1.5 m camera. Films were set with the incident beam parallel to the film surface (edge configuration), and SAXS profiles in the direction parallel to the film normal were measured with a one-dimensional position-sensitive proportional counter (PSPC). SAXS profiles were corrected for air scattering, specimen absorption, and thermal diffuse scattering (TDS) but not for slit smearing. The reliability of the data was carefully checked to confirm that the proximity of the beam stop did not affect the profile at low q values. In all cases, the first-order peak was found reasonably far away from the beam stop.

Samples were placed in a heating cell filled with nitrogen gas to avoid thermal degradation. SAXS profiles were measured in situ at varying temperatures. For each temperature of measurement, the samples were first preheated for at least 45 min to ensure thermal equilibration, and then subjected to SAXS measurements for 30 min. Average heating and cooling rates were 25 and 8 °C/h, respectively.

II.5. DMA. DMA was performed with a TA DMA2980 apparatus under dynamic tensile elongation unless otherwise stated. Temperature sweeps were conducted at a constant heating rate of 2 °C/min and at a constant frequency (1 Hz).

III. Results

Let us first briefly define the terminology used in this work. We adopted the traditional nomenclature used in the field of block copolymers. Under certain conditions, block copolymers self-assemble into ordered structures. The segregation process itself is conventionally called "microphase separation", while the domains constituting these ordered structures are called "microdomains". In mixtures of block copolymers having different block lengths or composition, some phase separation on macroscopic scales can occur. This phase separation is referred to as "macroscopic phase separation".

III.1. SBM Triblock Terpolymer $S_{22}B_{39}M_{39}{}^{41}$. III.1.1. Morphology in Ethylbenzene-Cast Films. The SAXS profiles given in Figure 2 show the morphological changes induced by annealing films that were cast from an ethylbenzene solution. Scattered intensity, I, multiplied by the Lorentz factor, q^2, is plotted as a function of the scattering vector, $q \equiv (4\pi/\lambda)\sin(\theta/2)$, λ and θ being the wavelength of the X-ray and the scattering angle, respectively. Before annealing, the as-cast morphology is not clearly defined. The profile of the as-cast film at 30 °C consists of only two broad maxima corresponding to a characteristic length, d, of about 21 nm. Here, it would not be appropriate to say that d corresponds to a lamellar long period since it is not clear that the morphology is lamellar. Accordingly, TEM observations reveal a poorly ordered morphology as shown in Figure 3a. Both a cylindrical morphology and a lamellar morphology seem to coexist. In some regions such as the inset of Figure 3a, one may see a cylindrical

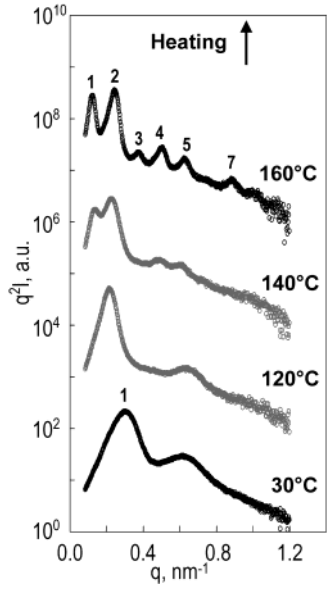

Figure 2. Evolution of SAXS profiles during heating from 30 to 160 °C for the ethylbenzene-cast $S_{22}B_{39}M_{39}^{41}$. Bold numbers indicate the order of the scattering maxima.

structure: S and M would form bright cylinders standing perpendicularly to the surface of the ultrathin film, while B stained with OsO_4 would be the dark matrix. In other parts of the TEM image (Figure 3a), cylinders seem to be interconnected to form lamellae. Such a morphology could correspond to an intermediate state quenched during a transition from a cylindrical to a lamellar structure. Indeed, similar TEM images have already been reported by Sakurai et al. for cylinder to lamella transition in the case of SBS triblock copolymers.[18]

Contrast in the TEM images is not sufficient to distinguish unambiguously S and M microdomains. Hence, we use DMA measurements to determine whether S and M are mixed or well-separated into distinct microdomains. Temperature dependence of the real part of the dynamic tensile modulus, E', and the loss tangent, tan δ, are shown in Figure 4a. Three different peaks in tan δ at −84, 104, and 134 °C clearly indicate the glass transition temperatures T_{gB}, T_{gS}, and T_{gM} of the three blocks B, S, and M, respectively, suggesting that the structure is made of well-separated S-, B-, and M-rich microdomains. Indeed, if S and M blocks were uniformly mixed into the same microdomains, there would have been a common glass transition for S and M. However, one should qualify this conclusion because the values measured by DMA for T_{gS} and T_{gM} are still different from those reported in Table 1. The heating ramp applied during the DMA measurement could have induced some microphase separation between S and M.

As mentioned in the Materials, the as-cast morphology is quite stable until 120−130 °C as shown in Figure 2 (120 °C). The scattering profile is only slightly shifted toward lower q values, and d increases from 21 nm (30 °C) to 29 nm (120 °C). After annealing above T_{gM} (from 140 °C), some major changes in the SAXS profile indicate that the morphology undergoes an important transformation. Several scattering maxima gradually appear. Ultimately, the profile after annealing at 160 °C exhibits many high-order scattering maxima (up to the seventh order at least) which are all located at integer multiples of the first-order peak position. This is the characteristic diffraction pattern of a lamellar

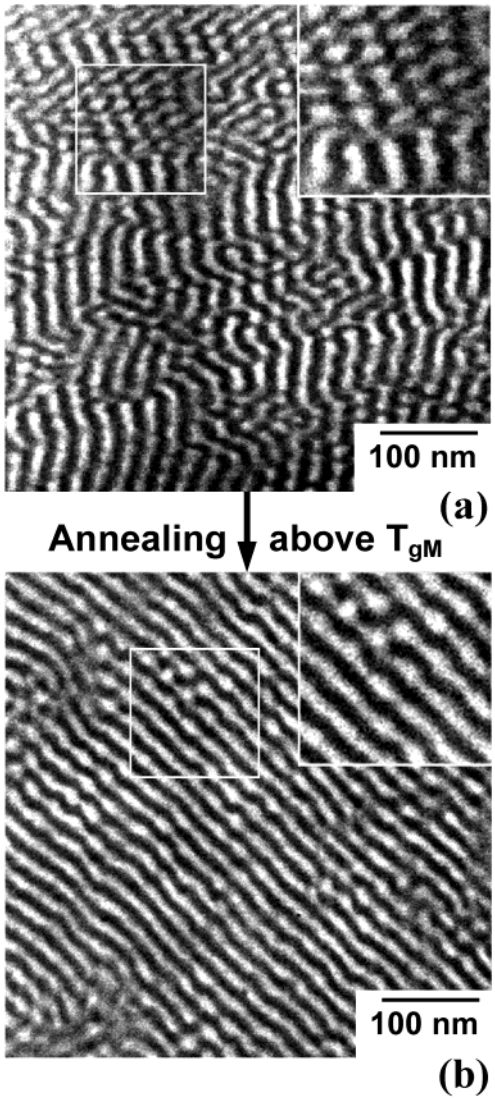

Figure 3. TEM images of ethylbenzene-cast films of $S_{22}B_{39}M_{39}^{41}$ stained with OsO_4 vapor, before (a) and after (b) annealing above T_{gM}.

morphology with an estimated lamellar long period, d_{001}, of 50 nm.

TEM images are consistent with the lamellar morphology deduced from SAXS measurements. After annealing, the as-cast morphology was transformed into a well-defined lamellar structure as shown in Figure 3b. This annealed morphology is more regular and extends over larger length scales compared to the initial as-cast morphology. In some parts of the TEM images, periodic variations of the lamellar thickness still remain as a memory of the cylindrical structure. As for the as-cast structure, the contrast in the TEM images is too weak to distinguish unambiguously the S and M microdomains. However, the lamellar long period estimated from TEM images would be about 40 nm if S and M were well-separated, while it would be 20 nm if they were mixed in common microdomains. Given that d_{001} measured by SAXS is 50 nm, the annealed morphology is most probably a completely segregated structure with distinct S-, B-, and M-rich lamellar microdomains.

DMA results in Figure 4b reveal distinct glass transitions for each of the three components, confirming as well that S, B, and M are well-separated into different microdomains. A comparison of the loss tangent data

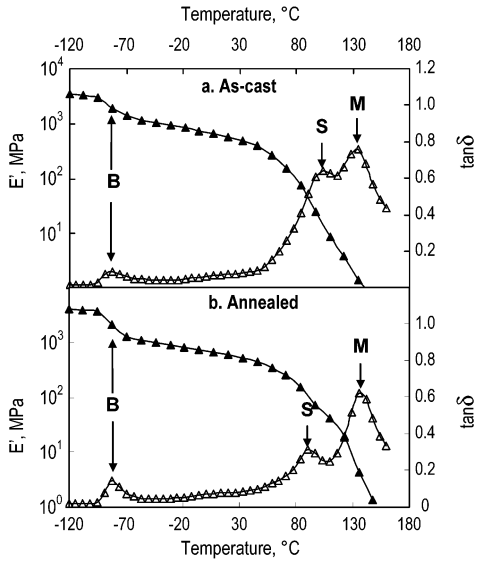

Figure 4. Temperature dependence of the real part of the dynamic elastic tensile modulus, E' (▲), and the loss tangent, tan δ (△), of ethylbenzene-cast films of $S_{22}B_{39}M_{39}{}^{41}$ before (a) and after (b) annealing above T_{gM} (f = 1 Hz, heating rate 2 °C/min).

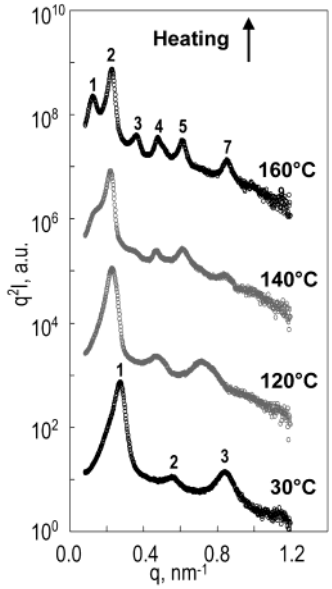

Figure 5. Evolution of SAXS profiles during heating from 30 to 160 °C for the chloroform-cast $S_{22}B_{39}M_{39}{}^{41}$. Bold numbers indicate the order of the scattering maxima.

also shows that microphase separation among S, B, and M is more pronounced in the annealed film than in the as-cast film. This difference between the as-cast and the annealed morphologies as well as the approximate doubling of the spacing revealed by SAXS strongly suggests that S and M are mixed or at least partially mixed in the as-cast state.

III.1.2. Morphology in Chloroform-Cast Films. The films cast from chloroform exhibit a well-defined lamellar morphology as shown by both SAXS and TEM. The SAXS profile of the as-cast morphology measured at 30 °C is given in Figure 5. It corresponds to a lamellar structure with up to four scattering maxima located at integer multiples of the first-order maximum position. d_{001} deduced from the peak positions is about 23 nm.

TEM images show a very regular lamellar morphology as illustrated in Figure 6a. In these images, well-defined

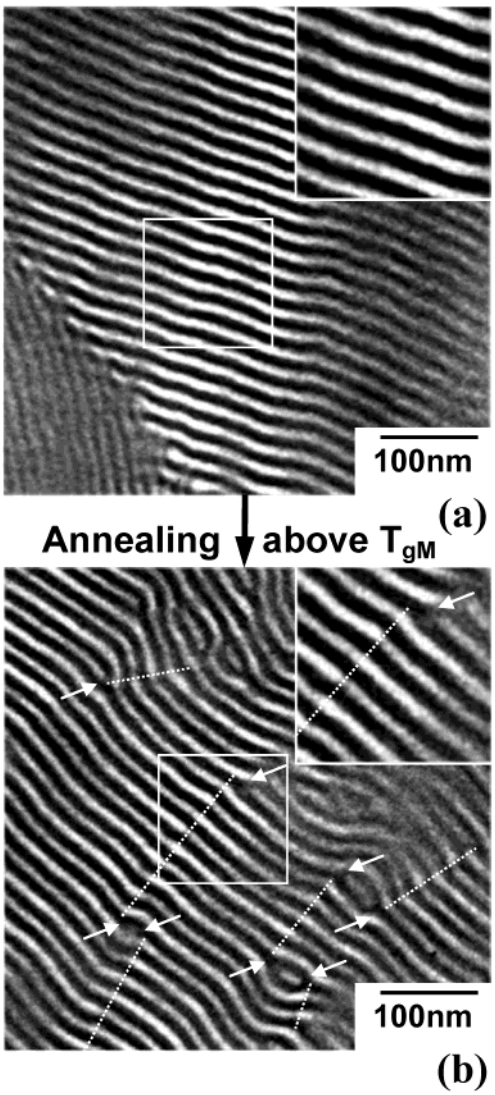

Figure 6. TEM images of chloroform-cast films of $S_{22}B_{39}M_{39}{}^{41}$ stained with OsO_4 vapor, before (a) and after (b) annealing above T_{gM}. Type 1 (S/M interfaces) and type 2 (dislocation-like) defects are indicated by dotted lines and white arrows, respectively.

dark lamellae are B-rich lamellar microdomains stained by OsO_4. In principle, when stained with OsO_4, S microdomains appear gray while M microdomains are brighter. The origin of this contrast difference is described later in this section. However, in the present case, S and M lamellae cannot be unequivocally distinguished. This may infer that the bright lamellae actually correspond to microdomains where S and M blocks are mixed. d_{001} measured by SAXS supports this idea. Indeed, one would have expected a much bigger value for d_{001} if S and M were well-separated. DMA results shown in Figure 7 are also consistent with this implication. Indeed, a single peak in tan δ located at an intermediate temperature (137 °C) between T_{gS} and T_{gM} strongly suggests the mixing of the S and M blocks in common microdomains. These DMA results are very similar to those by Yu et al., who reported phase mixing of S and M blocks in MSBSM pentablock copolymers.[19] Hence, all TEM, SAXS, and DMA experiments show that the chloroform-cast morphology consists of a partially mixed lamellar structure made of alternating B-rich and mixed S- and M-rich lamellar microdomains.

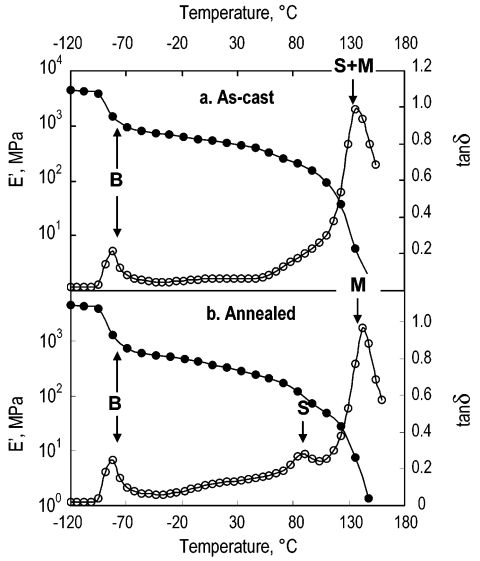

Figure 7. Temperature dependence of the real part of the dynamic elastic tensile modulus, E' (●), and the loss tangent, tan δ (○), of chloroform-cast films $S_{22}B_{39}M_{39}{}^{41}$ before (a) and after (b) annealing above T_{gM} (f = 1 Hz, heating rate 2 °C/min).

As for ethylbenzene-cast films, the chloroform as-cast morphology is quite unaffected up to 120−130 °C as shown by the SAXS profiles in Figure 5. From 140 °C, the SAXS profile is greatly changed, which reveals some important morphological transformation. Several new scattering maxima appear. At 160 °C, the resulting SAXS profile is very similar to that of annealed ethylbenzene-cast films with seven scattering maxima located at integer multiples of the first-order maximum. Such a profile corresponds to a lamellar structure with an estimated d_{001} of 52 nm.

In Figure 6b, TEM images of annealed chloroform-cast films also clearly show a lamellar morphology. However, alternating gray and bright lamellae indicate that S and M are now separated into distinct microdomains. This is consistent with the value of 52 nm for d_{001} measured by SAXS. Indeed, this value is twice that of d_{001} in the as-cast structure where S and M were mixed. In the TEM images, gray lamellae correspond to S-rich microdomains whereas bright lamellae are M-rich microdomains. This contrast difference between S and M is due to the degradation of the M blocks by the electron beam, which induces a thinning of the M microdomains along the normal to the ultrathin film surface.[5,20] This consideration provides hints to distinguish M and S lamellae. Unlike in the as-cast morphology, the annealed morphology exhibits many structural defects as highlighted by bright dotted lines and arrows in Figure 6b. These defects could be observed all over the ultrathin sections and for different samples. A few examples of high-magnification images are shown in Figure 8. One can classify these defects into two main categories that we will call defects of types 1 and 2, respectively. A scheme illustrating the two types of defects and the precursor of the type 2 defect is presented in Figure 9.

Defects of type 1 can be identified thanks to a characteristic S/M interface which determines S and M regions within the same layer sandwiched between two B lamellae (see Figure 9). In other words, a sequence of SBMB lamellae is connected to an MBSB sequence across a defect wall where S (respectively M) is in contact with M (respectively S) and B lamellae are continuous. Such interfaces are highlighted with white dotted lines in TEM images in Figure 6b and Figure 8. In Figure 8 where there is a good contrast between S and M, these defect walls appear very clearly. They seem to delimitate boundaries between grains which have shifted sequences of MBSB and SBMB lamellae.

Defects of type 2 look like dislocations. Some of them are indicated by white arrows in Figure 6b and white circles or rectangles in Figure 8. They correspond either to the junction of two B lamellae (Figure 8a,b, top of

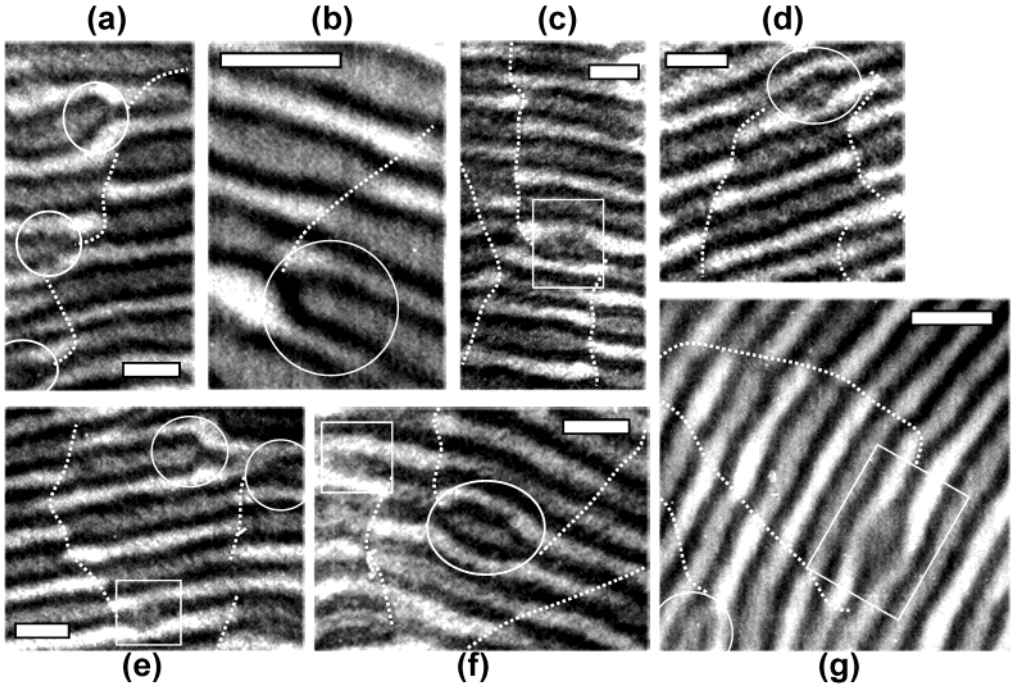

Figure 8. TEM images of morphological defects in annealed chloroform-cast films of $S_{22}B_{39}M_{39}{}^{41}$ stained with OsO_4 vapor. Dotted lines are drawn along the S/M interfaces (type 1 defects). Type 2 defects are framed with white circles or rectangles. Rectangles are used when the small S layer is only partially wrapped by a B layer. White bars correspond to 50 nm.

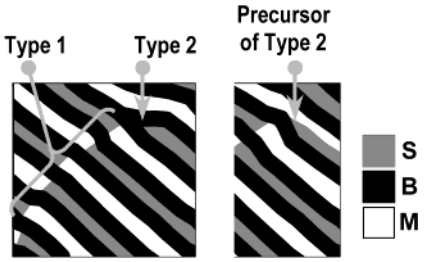

Figure 9. Schemes representing type 1 and 2 defects as well as the precursor of type 2 defects observed in Figure 6.

Figure 8e) or to a small additional S layer which can be completely (circles) or partially (rectangles) wrapped by B layers (Figure 8c−g). As will be suggested later in the Discussion, partially wrapped defects (rectangles) may actually be intermediate states (precursors) in the defect-formation process that ultimately results in completely wrapped defects (circles). A closer observation of the TEM images shows that type 2 defects are most often coupled with type 1 defects in the following way: the junction of two B lamellae seems to be the starting or ending point of S/M interfaces which extend across several lamellae. We will discuss the formation of these defects and explain the origin of this particular feature later in this paper.

The separation of S and M blocks is also confirmed by DMA as shown in Figure 7. Indeed, at high temperatures, two successive drops in E' and two peaks in tan δ at 90 and 144 °C reveal the glass transitions of the S and M microdomains, respectively. These two glass transition temperatures are close to the values measured in an SBM lamellar system, which is known to be completely segregated (see Table 1).

III.2. SBM Triblock and SB Diblock Mixture, an SBM/SB Blend. The chloroform-cast SBM/SB blend exhibits a completely segregated lamellar morphology with alternating S-rich (gray), B-rich (dark), and M-rich (bright) lamellae as shown in the TEM images in Figure 10a,b. Lamellae are very regular and form large grains extending over several micrometers. Bright spots in Figure 10a are due to impurities trapped in the film. Estimations of the lamellar spacing, d_{001}, from TEM images give an approximate value of 35 nm.

The corresponding SAXS profile is given in Figure 11 (as-cast profile). Like TEM images, this SAXS profile is consistent with a well-separated lamellar morphology for the following reasons. One can recognize the characteristic profile of a lamellar structure with up to nine orders of scattering maxima located at integer multiples of the first-order peak position. The scattering vector for the first-order maximum, q_{001}, was determined by Bragg's law from the position of the high-order diffractions from (002) to (007). The so-measured value of q_{001} is 0.136 nm^{-1}, which corresponds to a d_{001} of 46 nm. This value is in relatively good agreement with the very

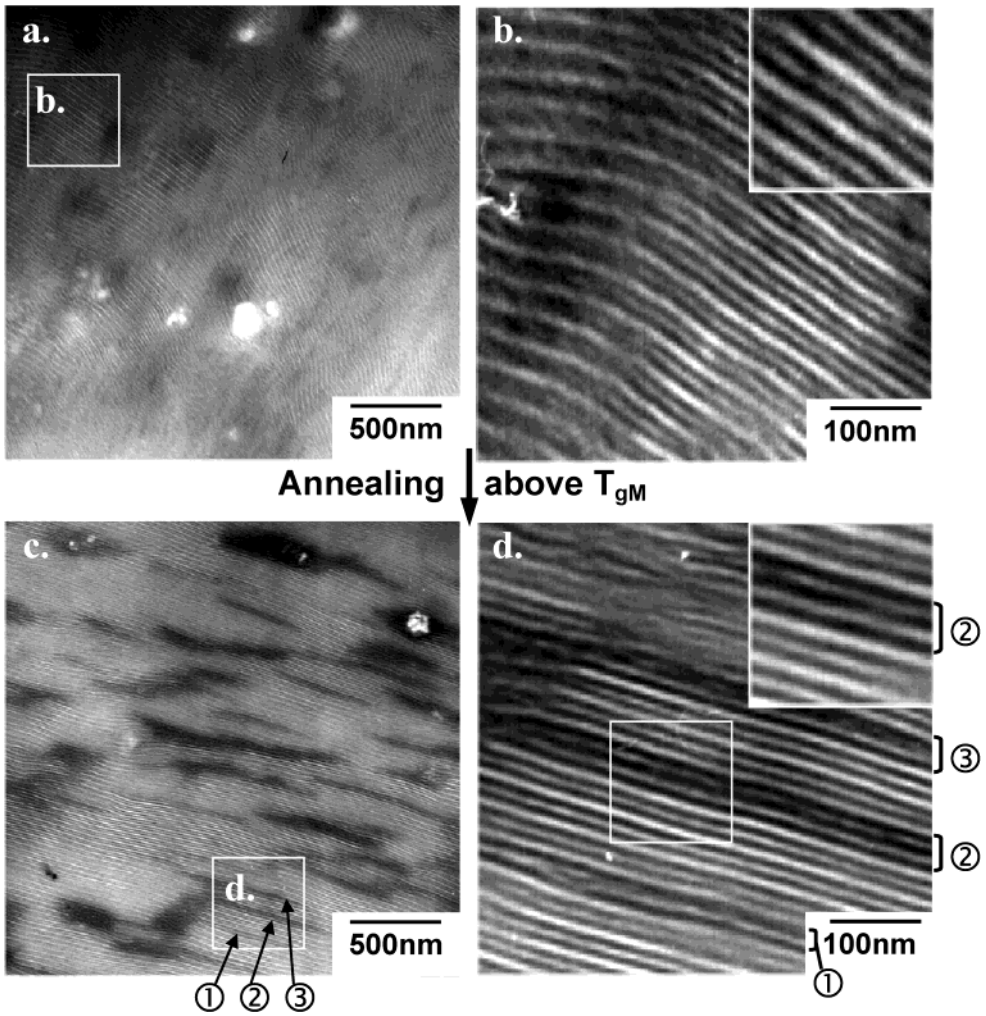

Figure 10. TEM images of chloroform-cast films of the SBM/SB blend stained with OsO_4 vapor, before (a, b) and after (c, d) annealing above T_{gM}. Part of the picture is zoomed (×1.5) in the top right corner of images b and d.

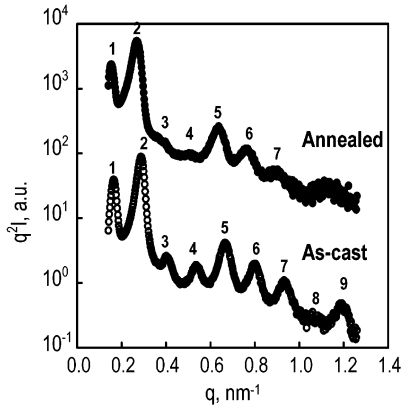

Figure 11. SAXS profiles of chloroform-cast films of the SBM/SB blend before and after annealing above T_{gM}. Bold numbers indicate the order of the scattering maxima.

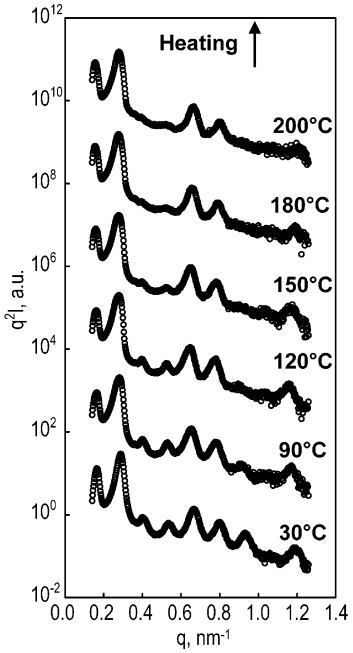

Figure 12. Evolution of SAXS profiles during heating from 30 to 200 °C for the chloroform-cast SBM/SB blend.

rough estimation made from TEM images. This seems to confirm the existence of three distinct types of microdomains.[21] The fact that TEM images give a lower value for d_{001} than SAXS measurements is probably due to a shrinkage of the M microdomains under the electron beam. It is also interesting to notice that the intensity of the second-order peak is close to the intensity of the first-order peak. Tanaka et al. argued that such a high intensity of the (002) reflection, never observed in systems with only two kinds of microdomains, can be explained by the q dependence of the form factor in lamellar systems having three different microdomains.[6]

Interestingly, the slow heating of the sample up to 200 °C does not induce major changes in the structure. Figure 12 shows the SAXS profiles measured during the heating for the chloroform-cast blend SBM/SB. Clearly, it is impossible to attain the order−disorder transition. The SAXS profile for the annealed specimen shown in Figure 11 was obtained after the sample was slowly cooled from 200 °C to room temperature. It corresponds to a lamellar structure similar to that of the as-cast film. The periodicity changes slightly, and the peaks are shifted toward smaller q values with increasing temperature. However, this shift is small since the long period for the annealed sample is about 48 nm, almost equal to the 46 nm measured in as-cast films. High-order diffraction peaks are also broader and less intense than for the as-cast profile. We attribute this effect to the macroscopic phase separation of the SB diblock upon annealing as will be detailed below. In conclusion, despite these slight changes, the blend is found to be thermally very stable, no major changes occurring during various thermal treatments.

TEM images of the annealed morphology, given in Figure 10c,d, also confirm a completely segregated lamellar morphology made of alternating S, B, and M lamellae. However, these images reveal the appearance of dark domains that could not be observed in the initial as-cast morphology. After a closer inspection, these dark domains are identified as SB diblock macrodomains made of alternating S and B lamellae inserted between SBM lamellae. Since the SB diblock is richer in B than SBM (64 wt % versus 39 wt %), SB domains look darker than SBM domains when stained with osmium tetroxide. The TEM image in Figure 10d is obtained by enlarging the portion enclosed by the white square in Figure 10c. It is focused on phase-separated SB diblock domains inserted between SBM lamellae. Dark grains indicated by marks 1 to 3 in Figure 10c actually correspond to S and B lamellae of SB diblocks inserted between M lamellae of the SBM structure. The size and shape of SB domains will be discussed in more detail in the Discussion.

Results for ethylbenzene-cast SBM/SB blend are not shown here. Both TEM and SAXS measurements show that the as-cast films have very poorly ordered morphologies. No macroscopic phase separation between SB and SBM could be observed. However, upon annealing above T_{gM}, the morphology changes into the same completely segregated lamellar morphology as for annealed chloroform-cast films. Hence, we are tempted to conclude that this completely segregated lamellar structure might be an equilibrium structure above T_g of the three blocks.

IV. Discussion

IV.1. Equilibrium Morphology in the Melt $S_{22}B_{39}M_{39}$[41]. Studies of block copolymers in solution show that, at some point of solvent evaporation, some of the components usually become glassy, preventing total thermal equilibration of the structure.[22−24] Hence, as-cast morphologies are more or less quenched copolymer solution morphologies and can be very different from the equilibrium structure of the melt copolymer (provided that one could ever obtain such a structure). In the present case, the equilibrium structure in the melt $S_{22}B_{39}M_{39}$[41] is most probably a lamellar morphology with well-separated S-, B-, and M-rich lamellar microdomains. Indeed, upon annealing, both ethylbenzene and chloroform-cast morphologies change into the same completely segregated lamellar morphology. This conclusion is consistent with the phase diagram of SBM triblock terpolymers reported by Stadler et al.[3] The as-cast morphologies and solvent effects observed here are also similar to those reported by Brinkmann et al. on not very different low molar mass SBM terpolymers.[9]

Both ethylbenzene and chloroform are rather good solvents of each block of the SBM copolymer and particularly of the S and M blocks. Hence, in solutions,

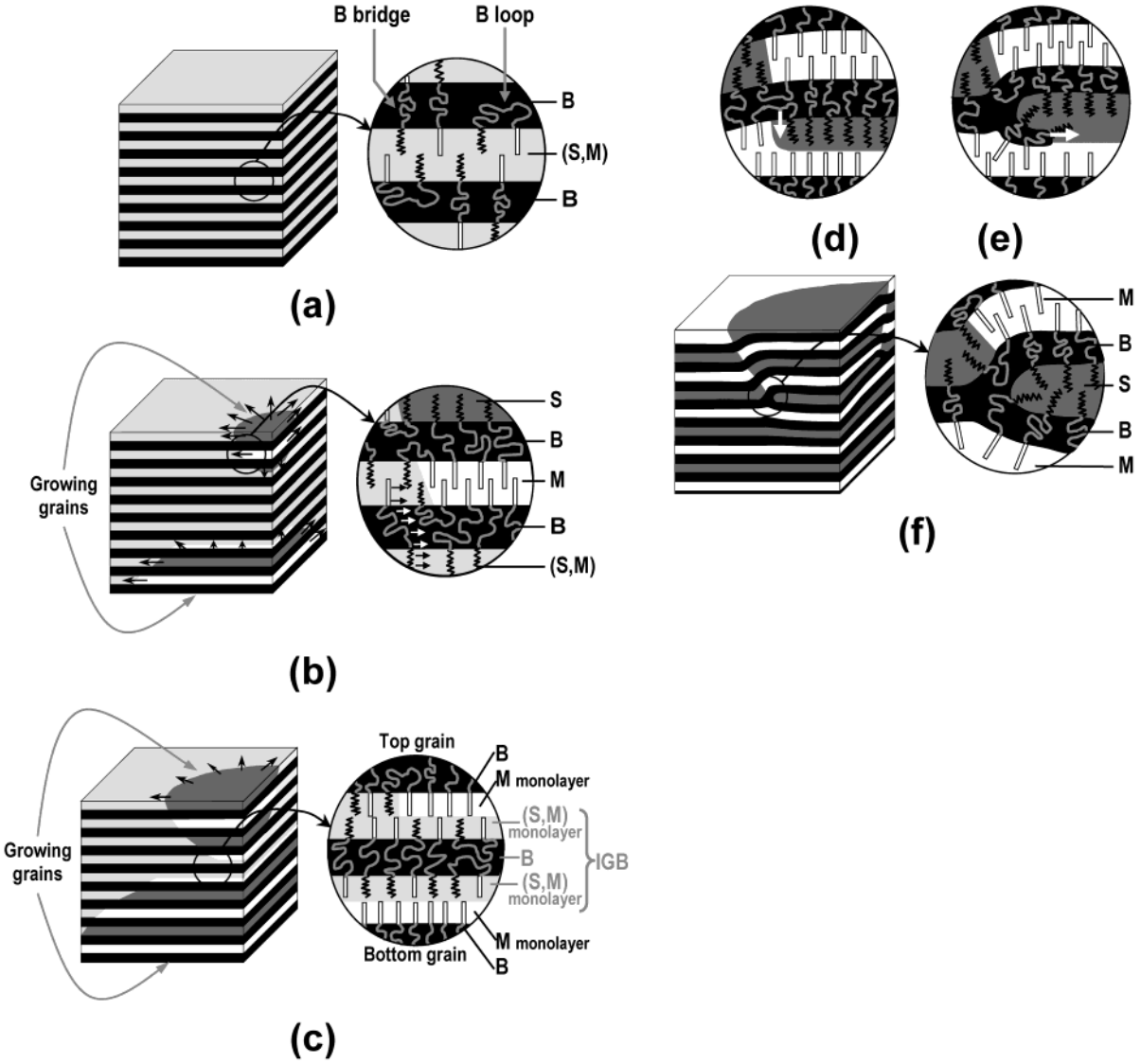

Figure 13. Description of the microphase separation mechanisms between S and M induced by annealing chloroform-cast $S_{22}B_{39}M_{39}$[41]. Annealing induces a transition from the partially mixed lamellar structure (a) to the completely segregated lamellar structure with trapped defects (f). (d) and (e) illustrate the detailed formation mechanisms of type 2 defects.

these solvents would consequently reduce repulsive interactions between the S and M blocks. The gain of mixing entropy at the interface with B could be high enough to favor a partially mixed lamellar structure over a completely segregated one.[26] Additionally, the effects of the casting solvent on copolymer morphologies can be rationalized by differences in solvent quality and selectivity. Indeed, ethylbenzene is a slightly better solvent for B than chloroform. Solubility parameters can be estimated to be $\delta_B \approx 8.3(\text{cal/cm}^3)^{1/2}$, $\delta_S \approx 9.1(\text{cal/cm}^3)^{1/2}$, $\delta_M \approx 9.3(\text{cal/cm}^3)^{1/2}$, $\delta_{\text{chloroform}} \approx 9.3(\text{cal/cm}^3)^{1/2}$, and $\delta_{\text{ethylbenzene}} \approx 8.8(\text{cal/cm}^3)^{1/2}$.[3,25] As a consequence, compared to chloroform, ethylbenzene would swell more the B microdomains than the microdomains made of mixed S and M. This slight selectivity could explain the asymmetry that produces a quite cylindrical morphology in films cast from ethylbenzene with cylinders of mixed S and M in a B matrix rather than a lamellar morphology made of alternating B and mixed S and M lamellae as in films cast from chloroform. Cylindrical structures could be expected in the melt for copolymers having a higher B volume fraction.[27]

The above considerations are quite speculative since the solvent effects anticipated here are relatively subtle. At this point, it is also particularly difficult to assess precisely when exactly the system is quenched during solvent evaporation. Exploration of morphologies in solutions at various concentrations might deserve a detailed separate study. Here, we focus on the mechanisms of morphological equilibration induced by annealing.

IV.2. Separation Mechanisms of S and M upon Annealing. According to this work, the samples cast from ethylbenzene exhibit poorly ordered morphologies where S and M might be mixed. As a result, it is difficult to interpret precisely the morphological changes occurring during annealing. Thickness fluctuations of the lamellae remaining after annealing might only be considered as nonequilibrium memory effects.

The case of chloroform-cast films is clearly much more interesting. As reported previously in section III, annealing induces a transition from a lamellar state with mixed S and M blocks to a completely segregated state with alternating S, B, and M lamellae. This results from a microphase separation of the S and M blocks within the lamellar structure. The effective repulsion between S and M monomers might indeed lead to such a transition. It can be compared to the macroscopic phase separation within lamellae of mixed B and C blocks

found in mixtures of AB and AC diblock copolymers.[28] In the latter case, the macroscopic phase separation occurs thanks to a two-dimensional diffusion of the junction points along the lamellar interfaces. However, the present case is different since it deals with ABC triblock chains. Unlike mixtures of AB and AC diblocks, the junction points at both ends of the B block in ABC triblock chains must move cooperatively along the interfaces. Here, we propose a scenario describing S and M separation which could explain the origin of the defects observed in section III. The schemes in Figure 13 illustrate the different steps of the proposed separation process. Circular insets on the right-hand side of these schemes give an idea of the configuration of the chains. This scenario is based on three assumptions.

(i) In the as-cast film, both B loops and B bridges are present as illustrated in the inset of Figure 13a. Indeed, as mentioned before in section IV.1, in a chloroform solution, microdomains made of mixed S and M are favored because the tendency of S and M blocks to segregate is low. The dynamics and driving forces of the transition from partially to completely segregated three-component structures have already been observed by Cloître et al. in systems of the SBM triblock with oil or solvent.[10,11] By varying the concentration of the copolymer, the authors could induce the microphase separation between the S and M end blocks.

(ii) Because of high incompatibility of B with S and M, permeation of S and M blocks through the B lamellae is strongly inhibited. The potential barriers for such diffusion across a B layer can be estimated to be very high. This approximation is based on and consistent with studies of diffusion of diblock chains in a lamellar structure.[12−15]

(iii) Thanks to the low molar mass, blocks are expected to be only slightly entangled and the in-plane diffusion of the chains should then be reasonably fast for the experimental time scale.

The lamellar structure which is quenched in the initial as-cast state consists of alternating layers of B blocks and of mixed S and M blocks. The layer thickness as estimated from TEM micrographs suggests that these mixed layers are actually bilayers composed of both S and M blocks mixed together (Figure 13a). In what follows, we denote such mixed layers by (S,M). When the sample is annealed above the glass transition temperatures, T_{gS} and T_{gM}, chain mobility is greatly enhanced. The microphase separation of S and M could then be described as follows. First, the S and M blocks tend to locally microphase separate due to effective repulsive interactions between S and M. The resulting microphase-separated regions grow by diffusion of the chains within the plane of the (S,M) bilayers. At both ends of the B blocks, the junction points with the S and M blocks move along the interface between the B and the (S,M) layers. However, this process is not a simple two-dimensional phenomenon because it cannot be confined in only one layer. Indeed, the (S,M) monolayers on both sides of a B lamella are connected by B bridges, as shown in the inset of Figure 13a. This connection by B bridges implies that the separation of S and M blocks in one (S,M) monolayer induces a cooperative reorganization in the neighboring (S,M) monolayer on the other side of the B lamella. Thus, the microphase separation propagates in all three directions, not only parallel to the lamellar interface but also perpendicular to it, as indicated by arrows in Figure 13b.

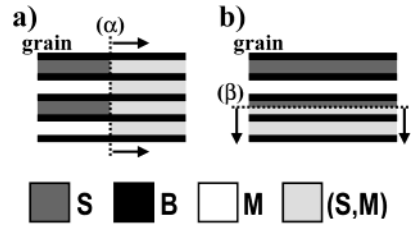

Figure 14. Schemes illustrating the two types of grain boundaries (α and *β*).

In the following discussion, a "grain" designates the completely segregated lamellar region made of well-separated alternating S, B, and M layers. Each grain is embedded and grows in the lamellar matrix where S and M are mixed as described above. An illustration of two grains in the matrix is sketched in Figure 13b: a small grain growing from the top and a big one from the bottom.

Due to the anisotropy of the lamellar structure, we must distinguish two types of grain boundaries as shown in Figure 14. Boundaries of type α (Figure 14a) are perpendicular to the lamellar interfaces and move parallel to them as the grain expands. On the contrary, boundaries of type *β* (Figure 14b) are parallel to the lamellar interfaces and move along their normal. The connections between the layers at these grain boundaries can be described as follows. At boundaries of type α, B layers extend continuously from the completely segregated to the partially mixed structure, while both bilayers of S and of M are connected to (S,M) bilayers. At boundaries of type *β*, the situation is different. The grains grow thanks to the B bridges that transmit the microphase separation from one (S,M) monolayer to the next neighboring (S,M) monolayer. Hence, at these boundaries, a monolayer of either S or M is interfaced with a mixed monolayer of (S,M). One should distinguish the notion of defect (types 1 and 2) from the notion of grain boundary (types α and *β*). Grain boundaries correspond to the interfaces between the completely segregated growing grains and the partially segregated matrix. On the other hand, defects refer to the structural imperfections observed in the completely segregated structure once the reorganization process has been completed.

As mentioned before and illustrated in Figure 13a, we expect that some of the B blocks form loops and link some S and M blocks that belong to the same monolayer. During the reorganization process, it is most probable that neither the S nor the M block can cross the B layers since both S and M are very incompatible with B. Without such a translayer permeation, the only way to separate S and M blocks is to expel the B loops to the grain boundaries of type α, as suggested in the inset of Figure 13b.

Grains like those in Figure 13b further grow in all three directions, and their expanding fronts ultimately come into contact along an intergrain boundary (IGB) as defined in the inset of Figure 13c. At this stage of the process, we need to distinguish two situations depending on the type of grain boundaries that come into contact as schematically represented in Figure 15.

In the first situation, the grains come into contact along boundaries of type α. If the sequence orders of the S, B, and M lamellae are the same in both grains (case i), the grains naturally merge into a bigger completely segregated lamellar region. However, an

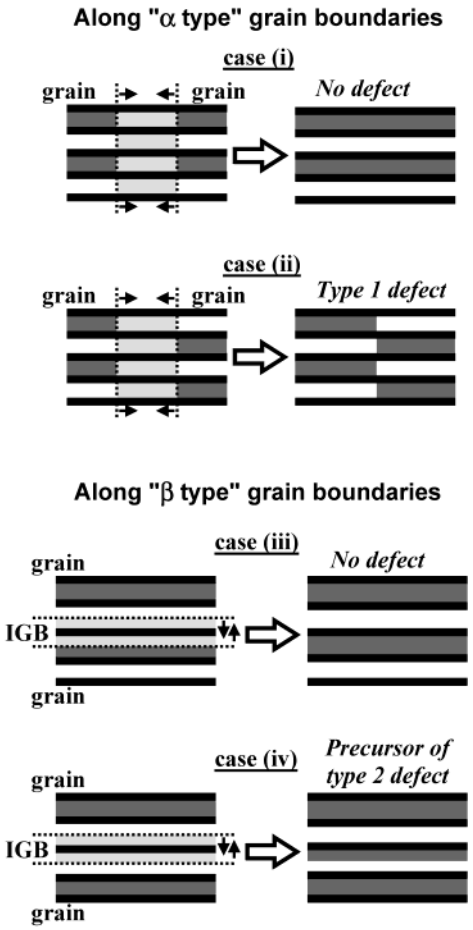

Figure 15. Schemes representing the four possible cases of intergrain boundaries before (left side) and after (right side) the welding of the grains: cases i and ii for grain boundaries of type α, and cases iii and iv for grain boundaries of type *β*. The legend is the same as in Figure 14.

intergrain boundary of finite thickness, not represented in Figure 15, may be left over as a defect region where B loops and hence (S,M) bilayers are condensed. On the contrary, if the sequence orders are shifted (case ii), the grains are welded along a defect wall of type 1 as previously described in section III. Here also, B loops and some (S,M) bilayers might be condensed along this defect wall. This may enable a smooth change in the layer thickness from the S to the M bilayers. Thus, this first situation along α-type boundaries can be at the origin of type 1 defects but cannot explain the formation of type 2 defects observed in TEM micrographs.

In the second situation represented in Figure 15, the grains come into contact along boundaries of type *β*. The IGB consists of a B layer covered on both sides by (S,M) monolayers. Here also, two cases denoted iii and iv must be considered depending on the nature of the monolayers above and below IGB. Case iii is quite simple. The monolayers above and below IGB are different. For instance, the top monolayer is made of M blocks and the bottom one of S blocks. As a result, when the S and M blocks separate in the IGB, the two grains are smoothly welded as in case i.

Case iv is more complex and is at the very origin of both types of defects described in section III. It is the case represented in Figure 13c−f. Unlike case iii, the monolayers at the grain boundaries on both sides of the IGB have the same nature. They are either both M monolayers as shown in Figure 15 or both S monolayers. As a consequence, the only way to separate the S and M blocks mixed in the two (S,M) monolayers of the IGB is to create an interface between an S and an M monolayer as shown in the right scheme of Figure 15. This configuration, which is also represented in Figure 13d, corresponds to a precursor of type 2 defects, which was shown earlier in Figure 9. It could be observed in several locations in the TEM images. Examples are framed with a rectangle in Figure 8c,e−g. However, such a configuration is energetically very unfavorable because the chains are strongly stretched to minimize the contact area between S and M blocks. This stretching could be released when SBM chains with a B loop diffuse along the S/M interface and wrap the S monolayer as indicated by bright arrows in Figure 13d,e. The presence of B loops is crucial here because quite unexpectedly, they would enable the formation of a new layer without permeation of the S and M blocks through a B lamella.

Eventually, "incompatible" grains can be connected by this new additional layer, forming defects of type 2 as shown in Figure 13f. Examples marked with a circle are shown in Figure 8. This would then be naturally followed by the creation of S/M interfaces (type 1 defects) as the grains grow further. It is interesting to notice that, according to this scenario, the concentration of B loops should be particularly high at S/M interfaces as suggested in the inset of Figure 13f. On the contrary, the creation of type 2 defects would enable B loops to change into B bridges during the microphase separation of S and M blocks. The B loops that might be condensed in the intergrain regions would be more or less effectively annihilated owing to this mechanism.

Interestingly, the defects reported in this work are very similar to the structural defects observed in ordered atomic systems. In some intermetallic compounds made of A, B, and C atoms, the unit cell consists of two different types of sites. One type of site is occupied by A atoms, while the other type is occupied by either B or C atoms. Hence, A atoms could correspond to the B blocks, and B and C atoms would play the role of the S and M blocks, respectively. In these systems, type 1 defects would correspond to antiphase boundaries while type 2 defects would be the partial dislocations bounding these antiphase boundaries.[29]

IV.3. Macroscopic Phase Separation in the Melt between SB and SBM. As for $S_{22}B_{39}M_{39}$[41], the samples of the SBM/SB blend cast from chloroform have an out of equilibrium structure. Indeed, SB diblock chains are completely incorporated into the SBM lamellar structure, whereas annealing induces an important macroscopic phase separation between SB and SBM chains. This is in good agreement with the experimental work of Abetz et al.[8] and theoretical work of Birshtein et al.[17] on mixtures of an ABC triblock and an AB or a BC diblock. In the case of lamellar structures where both triblock and diblock chains have the same block lengths, Birshtein et al. estimated that a mixture of an SB diblock and an SBM triblock always completely macrophase separates.

Among all the possible mixtures of an ABC triblock and an AB diblock, the low molar mass system studied here is quite specific. Indeed, rheological measurements (not shown here) on the pure SB diblock copolymer extracted from the blend show an order−disorder transition at about 176 °C (T_{ODT}). This is revealed by the sharp drop over a narrow temperature range of a few

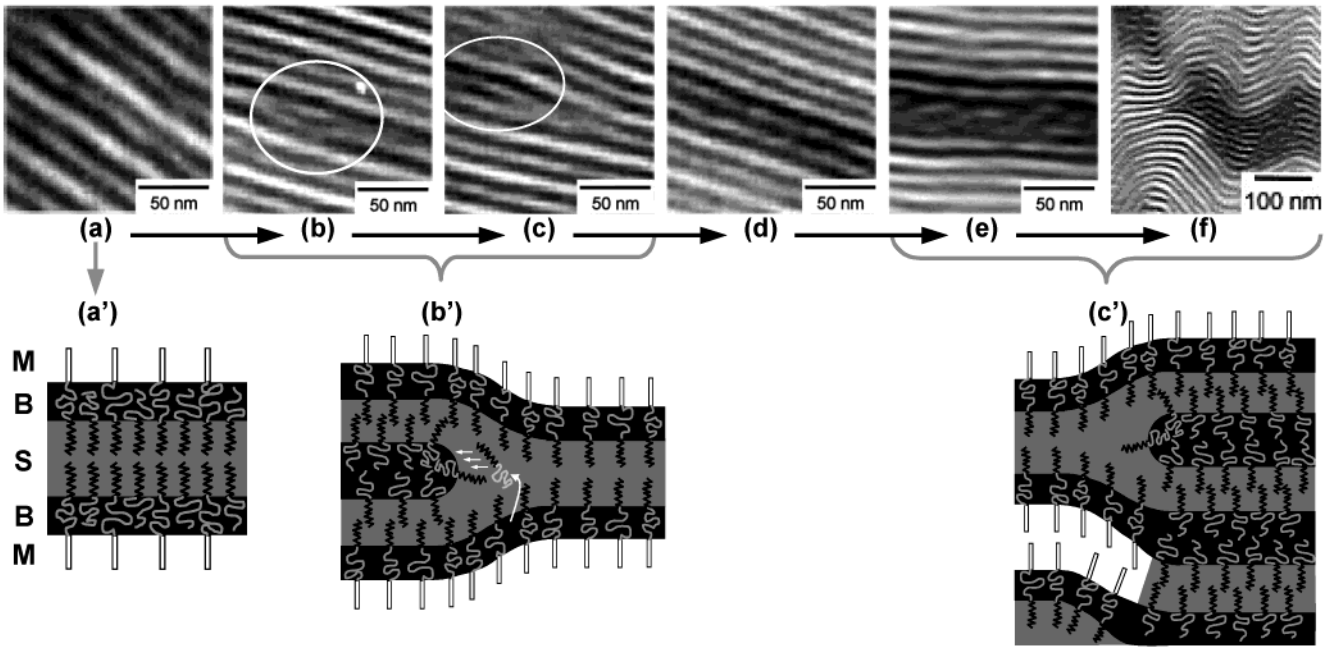

Figure 16. Description of the macroscopic phase separation in the melt between an SB diblock and an SBM triblock in the blend $S_{29}B_{47}M_{24}$. (a)−(f) are TEM images, while (a′)−(c′) represent the configuration of the chains: before (a′) and after (b′, c′) the macroscopic phase separation.

degrees by about 3 orders of magnitude in the dynamic elastic shear modulus measured at 0.1 rad/s.[30] This peculiarity of the SB diblock chains can probably explain their good incorporation into the SBM structure during solvent-casting. It might also facilitate the diffusion of the SB chains within the S and B lamellae during annealing.

A close observation of TEM micrographs of the annealed morphology enabled us to distinguish several types of SB diblock macrodomains differing in size and shape. Examples of each type are given in Figure 16b−f. Even though they all coexist in the same sample, we assume that these different types of macrodomains correspond to successive stages of the macroscopic phase separation process. Smaller macrodomains correspond to earlier stages. We can then propose a fairly intuitive scenario describing the steps and mechanisms of macroscopic phase separation. Before annealing, SB chains are fully incorporated in the SBM lamellar structure as shown in Figure 16a and schematically represented in Figure 16a′. This gives rise to a highly ordered lamellar morphology as manifested by up to at least nine orders of SAXS peaks in Figure 11. When the sample is annealed, diffusion of the SB chains becomes possible. As mentioned above, the structure with a homogeneously incorporated SB diblock is thermodynamically unstable. As for the microphase separation of S and M induced by annealing chloroform-cast $S_{22}B_{39}M_{39}$[41], a high potential barrier might prohibit permeation of SB chains through the M lamellae. Hence, SB diblock chains would phase separate by diffusing in the S and B lamellae. By analogy with blends of an AB diblock copolymer with an A homopolymer having the same length as the A block, the system might adopt a dry-brush-like configuration. The SB diblock would be expelled inside the S lamellae of the SBM structure and self-assemble, forming a new B lamella inserted in the middle of the S layer as shown in Figure 16b,c. This mechanism is probably favored when the annealing temperature is close to T_{ODT}. Indeed, the junction point of the SB chains can easily move away from the interface between the S and B lamellae. An illustration is given in Figure 16b′. In the last step represented by Figure 16e,f,c′, SB macrodomains would grow and merge to form bigger grains extending across several SBM lamellae. Since phase separation is confined in the SBM lamellar structure, the lamellae in SB grains would be forced to be parallel to SBM layers. The effects of the SB diblock macrodomains on the net scattering and on the distortion of the SBM lamellae explain the changes, especially the broadening of the higher order peaks, of the SAXS profiles upon annealing as shown in Figure 11. From Figure 12, it appears that the broadening of the peaks occurs around 150 °C, which can be related to T_{gM} (144 °C).

V. Conclusion

In the present paper we point out an interesting specificity of ABC triblock systems compared to AB or ABA block copolymers. For the latter, annealing usually enhances the regularity of morphologies and annihilate structural defects caused by preparation conditions.[31] In ABC triblock copolymers, we show that chain reorganization mechanisms in the melt are more complex due to the presence of a third component. On one hand, chain diffusion is strongly confined within the ordered structures, and permeation through the microdomains is almost impossible. On the other hand, B bridges connecting the microdomains correlate the reorganization in the A and C layers. In some cases such as those reported here, the only way to approach the equilibrium state and satisfy the severe constraints imposed by high-energy barriers is to form new defects. Hence, the efficiency of annealing mostly depends on the initial state. Once the defects are formed, they are strongly trapped and are probably impossible to suppress. We have discussed the mechanisms of formation of two types of such defects (types 1 and 2) in the case of lamellar structures. Similar phenomena most probably exist in other morphologies.

In practice, high molar masses are often desirable to achieve better mechanical properties. For long chains,

however, topological constraints and thermodynamic barriers for equilibration are huge and completely hinder chain diffusion during annealing. The choice of the solvent is then of crucial importance to attain the desired properties of triblock materials.

In the mixture of SBM and SB block copolymers, we observed a possibly advantageous effect of solvent to trap interesting morphologies. After solvent evaporation, diblock and triblock chains are uniformly mixed to form a very regular lamellar morphology. However, annealing induced an important phase separation on a macroscopic scale, confirming that the as-cast state was thermodynamically unstable. We have proposed a scenario explaining the mechanisms of such phase separation in the ordered melt. In the early stage of the process, SB chains would diffuse within the S and B lamellae and be expelled inside the S lamellae of the SBM structure to form macrodomains of the SB diblock. These mechanisms are probably specific to this low molar mass system where the SB diblock exhibits an order−disorder transition temperature very close to the annealing temperature. For higher molar masses, mixed structures may be trapped forever.

Acknowledgment. We acknowledge the technical assistance of P. Coupard at some stages of this work. L.C. is very thankful to the Laboratory of Polymer Mechanics in the Division of Polymer Physics for hospitality during his stay at Kyoto University, where most of the experimental work was performed. We also thank one of the reviewers for pointing out the interesting analogy with ordered atomic systems. Financial support by ATOFINA, CNRS, ESPCI, and Kyoto University is gratefully acknowledged. T.H. gratefully acknowledges financial support via a Grant-in-Aid for Scientific Research under Grant No. 12305060 (A) from the Japan Society for the Promotion of Science and from the 21st century COE Program for a United Approach to New Materials Science.

References and Notes

(1) Park, M.; Harrison, C.; Chaikin, P. M.; Register, R. A.; Adamson, D. H.. *Science* **1997**, *276*, 1401−1404.
(2) Thurn-Albrecht, T.; Schotter, J.; Kästle, G. A.; Emley, N.; Shibauchi, T.; Krusin-Elbaum, L.; Guarini, K.; Black, C. T.; Tuominen, M. T.; Russell, T. P. *Science* **2000**, *290*, 2126−2129.
(3) Stadler, R.; Auschra, C.; Beckmann, J.; Krappe, U.; Voigt-Martin, I.; Leibler, L. *Macromolecules* **1995**, *28*, 3080−3097.
(4) Zheng, W.; Wang, Z. G. *Macromolecules* **1995**, *28*, 7215−7223.
(5) Breiner, U.; Krappe, U.; Thomas, E. L.; Stadler, R. *Macromolecules* **1998**, *31*, 135−141.
(6) Tanaka, Y.; Hasegawa, H.; Hashimoto, T.; Ribbe, A.; Sugiyama, K.; Hirao, A.; Nakahama, S. *Polym. J.* **1999**, *31*, 989−994.
(7) Bates, F.; Fredrickson, G. *Phys. Today* **1999**, February, 32−38 and references therein.
(8) Abetz, V.; Goldacker, T. *Macromol. Rapid Commun.* **2000**, *21*, 16−34 and references therein.
(9) Brinkmann-Rengel, S.; Abetz, V.; Stadler, R.; Thomas, E. L. *Kautsch. Gummi Kunstst.* **1999**, *12*, 806−813.
(10) Fleury, C. Doctoral Thesis, Université Pierre et Marie Curie, 2001.
(11) Yamaguchi, D.; Cloitre, M. To be published.
(12) Barrat, J.-L.; Fredrickson, G. H. *Macromolecules* **1991**, *24*, 6378−6383.
(13) Ehlich, D.; Takenaka, M.; Okamoto, S.; Hashimoto, T. *Macromolecules* **1993**, *26*, 189−197.
(14) Ehlich, D.; Takenaka, M.; Hashimoto, T. *Macromolecules* **1993**, *26*, 492−498.
(15) Lodge, T. P.; Dalvi, M. C. *Phys. Rev. Lett.* **1995**, *75*, 657−660.
(16) Mourran, A.; Leibler, L.; Court, F. Unpublished results, 1997.
(17) Birshtein, T. M.; Zhulina, E. B.; Polotsky, A. A.; Abetz, V.; Stadler, R. *Macromol. Theory Simul.* **1999**, *8*, 151−160.
(18) Sakurai, S.; Momii, T.; Taie, K.; Shibayama, M.; Nomura, S.; Hashimoto, T. *Macromolecules* **1993**, *26*, 485−491.
(19) Yu, J. M.; Dubois, Ph.; Jérôme, R. *Macromolecules* **1997**, *30*, 4984−4994.
(20) TEM observations (not shown here) of unstained SBM show a contrast difference between poly(styrene) and poly(methyl methacrylate) induced by electron beam damage.
(21) As the three components are clearly well-segregated in this annealed sample, it was used as a reference to determine the glass transition temperatures which are reported in Table 1.
(22) Hashimoto, T.; Shibayama, M.; Kawai, H. *Macromolecules* **1983**, *16*, 1093−1101.
(23) Mori, K.; Hasegawa, H.; Hashimoto, T. *Polymer* **1990**, *31*, 2368−2376.
(24) Lodge, T. P.; Pudil, B.; Hanley, K. J. *Macromolecules* **2002**, *35*, 4707−4717.
(25) Brandrup J, Immergut EH. *Polymer Handbook*, 3rd ed.; Wiley-Interscience: New York, 1989.
(26) .Abetz, V.; Stadler, R.; Leibler, L. *Polym. Bull.* **1996**, *37*, 135−142.
(27) Brinkmann, S.; Stadler, R.; Thomas, E. L. *Macromolecules* **1998**, *31*, 6566−6572.
(28) Kimishima, K.; Jinnai, H.; Hashimoto, T. *Macromolecules* **1999**, *32*, 2585−2596.
(29) Gleiter, H *Physical Metallurgy*, 3rd ed.; Elsevier Science Publishers B.V.: Amsterdam, 1983.
(30) Rosedale, J. H.; Bates, F. S. *Macromolecules* **1990**, *23*, 2329−2338.
(31) Harrison, C.; Adamson, D. H.; Cheng, Z.; Sebastian, J. M.; Sethuraman, S.; Huse, D. A.; Register, R. A.; Chaikin, P. M. *Science* **2000**, *290*, 1558−1560.

MA034169J